A Novel and Low-Cost Sea Ice Mass Balance Buoy

KEITH JACKSON* AND JEREMY WILKINSON+

Scottish Association for Marine Science, Oban, United Kingdom

TED MAKSYM

Woods Hole Oceanographic Institution, Woods Hole, Massachusetts

DAVID MELDRUM

Scottish Association for Marine Science, Oban, United Kingdom

JUSTIN BECKERS AND CHRISTIAN HAAS

University of Alberta, Edmonton, Alberta, Canada

DAVID MACKENZIE

University of Oxford, Oxford, United Kingdom

(Manuscript received 7 March 2013, in final form 7 August 2013)

ABSTRACT

The understanding of sea ice mass balance processes requires continuous monitoring of the seasonal evolution of the ice thickness. While autonomous ice mass balance (IMB) buoys deployed over the past two decades have contributed to scientists' understanding of ice growth and decay processes, deployment has been limited, in part, by the cost of such systems. Routine, basinwide monitoring of the ice cover is realistically achievable through a network of reliable and affordable autonomous instrumentation. This paper describes the development of a novel autonomous platform and sensor that replaces the traditional thermistor strings for monitoring temperature profiles in the ice and snow using a chain of inexpensive digital temperature chip sensors linked by a single-wire data bus. By incorporating a heating element into each sensor, the instrument is capable of resolving material interfaces (e.g., air–snow and ice–ocean boundaries) even under isothermal conditions. The instrument is small, low cost, and easy to deploy. Field and laboratory tests of the sensor chain demonstrate that the technology can reliably resolve material boundaries to within a few centimeters. The discrimination between different media based on sensor thermal response is weak in some deployments and efforts to optimize the performance continue.

1. Introduction

This paper describes the development of a new ice mass balance (IMB) buoy that uses the established principle of measuring temperatures at closely spaced intervals down a chain of sensors deployed through sea ice. However, this new IMB buoy uses a novel construction method for the chain that allows opportunities for dramatic reduction in cost and complexity compared to previous thermistor chain designs. Also, we describe a heated anemometer mode that allows for identification of interfaces in isothermal conditions and potentially allows for additional information on air and water currents to be collected without requiring other sensors.

In addition to a technical description, we present examples of deployment results and describe ongoing development and characterization work.

* Current affiliation: Oceanlab, University of Aberdeen, Newburgh, Aberdeenshire, United Kingdom.

+ Current affiliation: British Antarctic Survey, Cambridge, United Kingdom.

Corresponding author address: Keith Jackson, Oceanlab, University of Aberdeen, Newburgh, Aberdeenshire AB41 6AA, United Kingdom.
E-mail: keith.jackson@abdn.ac.uk

DOI: 10.1175/JTECH-D-13-00058.1

For the purposes of this paper, we will refer to this new instrument as the Scottish Association for Marine Science (SAMS) IMB buoy to distinguish from other types of IMB devices.

2. Sea ice mass balance measurement

While satellites have monitored the state of the sea ice cover for over three decades, such techniques have only been able to provide information on the extent of the ice. Monitoring the thickness of the ice is a more difficult task. Radar and satellite altimetry are showing promise for large-scale monitoring of ice cover (e.g., Laxon et al. 2003; Kwok et al. 2004) but can only provide very broadscale estimates of ice thickness. Other techniques, such as drill-hole transects (e.g., Worby et al. 1996), airborne techniques (e.g., Kwok et al. 2012; Haas et al. 2010), and upward-looking sonar measurements of ice draft from submarines (Rothrock et al. 1999; Wadhams and Davis 2000; Rothrock et al. 2003), autonomous vehicles (Wilkinson et al. 2007), or moorings (Strass 1997), are capable of measuring the ice thickness distribution across various scales. However, none of these techniques is practical for monitoring the time evolution of the snow and ice thickness continuously throughout an annual cycle. Until the advent of IMB buoy technology, most of our understanding of time-dependent sea ice mass balance processes, such as snow deposition and melt or ice growth and decay, has been inferred from field experiments of limited duration. For a comprehensive understanding of the processes governing ice growth and decay, or to evaluate various process models (e.g., for determining ice–ocean energy exchange), it is necessary to monitor the snow and ice thickness distribution continuously. This has been done sporadically with hot-wire thickness gauges (Untersteiner 1961) and thermistor strings (Ackley et al. 1996). However, the only practical method for routine monitoring over long time periods (such as an entire annual cycle) or in marginal ice conditions is with autonomous instrumentation.

The first all year-round direct autonomous measurements were achieved with the Cold Regions Research and Engineering Laboratory (CRREL) ice mass balance buoys (Richter-Menge et al. 2006). The CRREL IMB buoy uses a thermistor chain to measure the temperature profile through the ice, typically at 5–10-cm intervals. Two acoustic sensors monitor mass balance—one mounted over the surface for snow accumulation or ablation and one under the ice to measure ice growth or melt. Data are transmitted via the Argos satellite system or, more recently, the Iridium system. A seasonal IMB buoy designed to survive the summer melt season has also been developed (Polashenski et al. 2011).

The CRREL IMB buoys have proved very successful in helping to elucidate details of annual sea ice evolution and surface melt. This has contributed to our understanding of the causes of the recent dramatic retreat of Arctic perennial ice (Perovich et al. 2008), and highlighted the differing processes governing sea ice mass balance in the Antarctic (Perovich et al. 2004). Despite its technical success and wide adoption over two decades by the scientific community for use in the Arctic, the number of deployments has been fairly limited, with only a handful having been deployed to date in the Antarctic. It seems likely that this has been partly because of the expense of an individual system and the logistical requirements of deployment. Potential sources of the expense are as follows:

1) The use of relatively expensive sonar sensors and associated structure for mounting and positioning.
2) Thermistor chains with a large number of thermistors, hence many wires and connections.
3) The Argos data costs are relatively high given the small message sizes typically transmitted.
4) The use of an expensive industry standard datalogger.

The work detailed in this paper was to modify the successful CRREL IMB buoy concept to permit more extensive deployments. This centered on the following criteria:

1) Low cost. The SAMS IMB buoy is approximately a one-quarter of the cost of a CRREL IMB buoy, meaning a larger number of buoys could be deployed for a given budget, allowing for better information on spatial variability of ice mass balance processes to be gathered.
2) Easy to deploy through a standard 2-in. auger hole by nonspecialists in minutes.
3) Data transmitted via Iridium, reducing costs and allowing the user total control of the data sampling strategy after initial deployment.
4) Custom-designed low-cost controller and logger.

These modifications to the IMB buoy concept were aimed at enabling a significant increase in the network size in both the Arctic and Antarctic, which in turn will deliver a better understanding of the mass balance evolution of sea ice and at higher spatial resolution than has been previously obtained.

Our cost comparison is based on the present sale price but this should be treated with caution, as the devices have been commercialized to different extents and use commerical models.

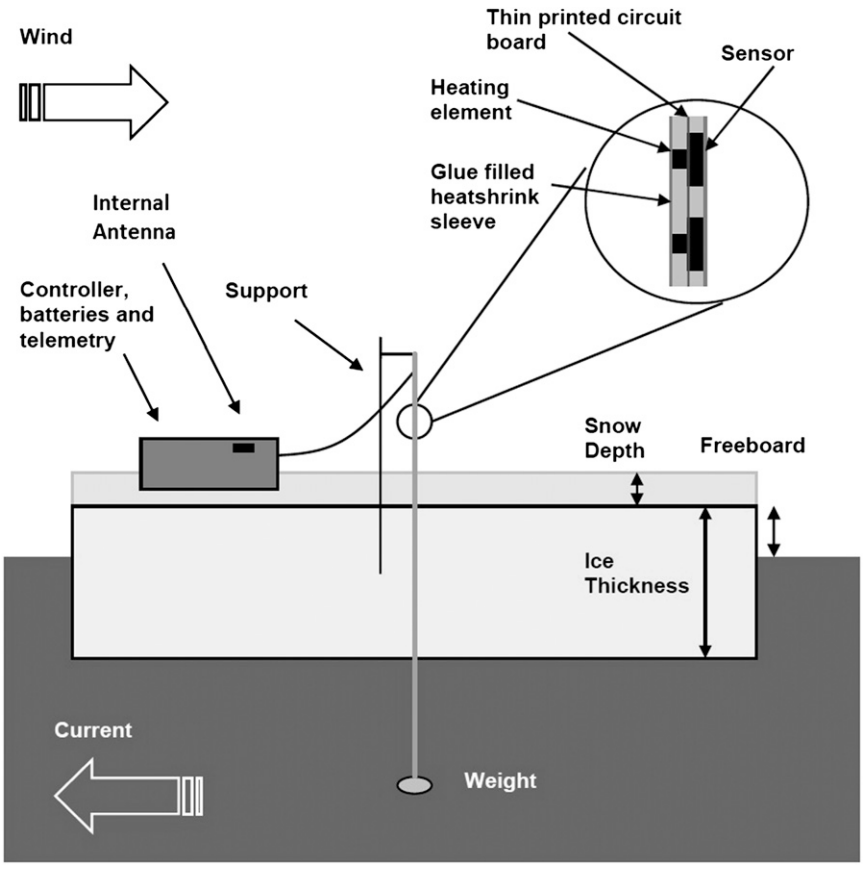

FIG. 1. Schematic of main system components in a typical deployment. The design consists of a sensor string lowered through a 2-in. drill hole through the ice and snow and connected to a small Pelican Case that houses electronics, batteries, and Iridium modem.

3. Technical description

A schematic showing the main components is presented in Fig. 1. Each major section is described in detail below.

a. Sensor chain

Thermistor chains have long been used for measuring temperature profiles within the upper ocean and sea ice (Mobley et al. 1976; Flower and Budgen 1987; Richter-Menge et al. 2006). All deployments have confronted similar problems, stemming from the complexity of both cable and connectors that results from the requirement to independently sample a large number of thermistors. Attempts have been made to minimize this complexity by replacing the analog thermistor element by a bus-addressable digital sensor module, but these have incurred penalties in both size and cost (Scott and McDowall 1990; Sellschopp 1997). Recent developments in sensor technology have led to a new type of bus-addressable digital temperature sensing integrated circuit (IC) that is both inexpensive and compact. Typically, these use an analog temperature sensing element that is interfaced to an on-chip digital control circuit. This allows control of the analog-to-digital conversion, storage of the result in memory, and digital communication over a common bus (Smith 2004). Critically, the number of cable cores required is reduced to just three (common power, data bus, and ground), regardless of the number of sensors used. These sensors are commonly used in the computer and automotive industries to provide temperature feedback in heating and cooling circuits. Each sensor device is assigned a unique identifier code at manufacture that can be used to address individual devices on a shared data bus.

We have constructed temperature measurement chains incorporating the type of sensors described above (specifically, the Maxim DS28EA00 device), which has significantly simplified cable and connector requirements, a huge benefit in terms of cost and reliability. The chains consist of 0.5-m sections of standard fiberglass printed circuit board (PCB) material (commonly referred to as FR4) but in a thickness of 0.2 mm instead of the usual

1.6 mm used for most PCBs. This makes for a flexible and light chain that is simple and durable enough for deployment in a 2-in. auger hole.

Sensors and other electronic components are attached using standard automatic placement and soldering techniques common in the electronics industry. Each section has etched copper tracks for interconnections, as is usual in PCBs, and each 0.5-m section can be joined at both ends to form a chain. The joint is formed by overlapping two ends that have corresponding holes and pads that are soldered together directly. Chain sections have been produced with 2-, 4-, or 50-cm sensor spacing, allowing chains to be tailored for particular applications. Typically, 2-cm-spaced sensors are now used for IMB buoys but larger spacing is used for applications such as monitoring of ocean mixed layer depth. The chain is connected by a cable to a microcontroller unit housed in an enclosure on the ice surface.

In addition to the three tracks running the length of the chain for power, ground, and data, a fourth track is used to power heater elements for the heating cycle mode. For each sensor, a resistor component is mounted immediately underneath the sensor on the opposite side of the PCB. An 8-V supply is connected to this track to cause gentle heating of each sensor and its surroundings. A 1-kΩ resistor gives rise to 64 mW of heating power per sensor, but this may be reduced if desired by pulse width modulation of the supply voltage. Low heating power may be used to avoid melting of ice and snow in contact with the chain as well as minimizing power requirements.

Additional wiring is also necessary between each adjacent sensor. Each sensor has a digital input and a digital output pin that are wired to the opposite pin type on the two adjacent sensors (i.e., input to previous chip output, output to subsequent chip input). This is necessary to allow identification of the order of the sensors on the chain using a ''daisy chain'' technique (Maxim Integrated 2007) that we now briefly describe. A command is broadcast from the controller on the single-wire bus that instructs all connected sensor chips to drive their output pin to a state rendering the next device in the chain inactive. The first sensor has its input hardwired to the active state. The controller can then interrogate the whole chain but only the first device will reply since all others are inactive. Its unique address can then be obtained by the controller without interference from other devices on the data line. Once this is done, the active device is instructed to drive its output pin to the active state and to become itself inactive until the whole chain is reset. The next interrogation of the chain then results in the second device on the chain responding. Repetition of the process allows for identification of each sensor on the chain in order of physical position. This whole process is automated in the controller software and takes less than a minute for a chain of 250 sensors. The addresses of the sensors in the order of their physical position are stored in a nonvolatile memory chip mounted at the top of each chain. This chip uses the same single-wire data bus as the sensors, and so no special wiring is needed and the controller can read it in the same manner as the sensors. This means that when a chain is plugged into a controller, the addresses of the devices and their order on the chain can be determined by interrogating the memory chip. Calibration data for the each sensor on the chain and a serial number are also stored in this memory.

To protect the sensors and PCB, the final chain assembly is threaded through a single length of glue-lined heat-shrink plastic sleeve that is then evacuated of air and baked to shrink the sleeve. The glue lining melts and flows freely around the enclosed components. On cooling the glue solidifies, leaving the sensors well sealed against water ingress and in good thermal contact with the external medium. The resulting chain of sensors is robust and durable and has a low thermal mass. White heat-shrink sleeve is used to minimize the possibility of solar heating of the sensors.

b. Controller

The controller is fairly typical of those used in similar autonomous systems. Early models of the SAMS IMB buoy used a Persistor CF2 logger (Persistor Instruments Inc. 2005) to perform control functions. This has now been replaced by a single-chip Microchip PIC (the original expansion of PIC is peripheral interface controller) microcontroller, resulting in significant cost savings and with no loss of performance or features. The specific device used was a PIC24FJ128GA106A (Microchip Technology Inc. 2010), which contains 128 kB of programmable, nonvolatile flash memory for the control program, 16 kB of RAM memory, and a comprehensive array of peripherals [e.g., universal asynchronous receiver/transmitter (UART), serial peripheral interface (SPI), inter IC (I^2C), real-time clock, and 12-channel 10-bit analog-to-digital converter (ADC)]. A LinkOEM one-wire bus interface unit (iButtonLink, LLC 2008) is used for communications with the sensors on the chain. This is controlled by the processor via a UART connection. An Iridium satellite modem using short-burst data (SBD) protocol is incorporated for telemetry. At present an Iridium 9602 SBD modem (Iridium Communications Inc. 2010) is used but the newer 9603 model (Iridium Satellite, LLC 2012) is being incorporated into future designs. The Iridium SBD system provides advantages over previous autonomous platforms that used the one-way Argos 2 system. With Iridium two-way communication

is available, and so it is possible to send instructions to the deployed device to modify the sampling regime or other operational parameters.

The controller incorporates all the necessary voltage regulation using linear devices. The heating mode uses 8 V and so a battery supply of 12–15 V is used. Most circuit elements require 3.3- or 5-V supplies and so linear voltage regulation is used to achieve this. However, linear regulation results in very inefficient use of battery power, and so it is anticipated that future versions will use switch-mode regulation to improve the efficiency. The controller is usually in a low-power dormant state (<300 μA) and is woken periodically by a real-time clock to perform tasks. Power is usually provided by 15-V alkaline D-cell packs. The battery life depends on the number of battery packs and the sample regime. With six battery packs, deployments of over a year are possible with GPS sampled hourly, temperature profiles every six hours and one heated profile daily. Battery voltages are communicated back periodically, and the sample regime can be adjusted remotely to manage battery life. Alkaline batteries exhibit an increase of internal resistance at very low temperatures, but the large number of packs connected in parallel reduces the effect of this and allows the unit to function down to -40°C. The entire system fits into a Pelican Case, with the total system weighing less than 14 kg. The lightest colors of case available are used to reduce heating from solar radiation.

A U-blox (formally Fastrax) UP501 GPS receiver (U-blox AG 2013) with integrated antenna is included to provide position information at much higher accuracy than Argos or Iridium satellite positioning. GPS accuracy is better than $\pm$10 m, whereas Argos accuracy is $\pm$150 m and Iridium is $\pm$10 km. The GPS data produced are useful for determining ice drift or, with multiple deployments in an array, ice deformation parameters.

The controller allows for a ''daughter board'' to be fitted on a set of headers. This allows for various additional sensors to be fitted without drastic redesign of the main PCB. Additional sensors that have been included are a MicroMag3 three-axis magnetometer to determine floe orientation (PNI Sensor Corp. 2010) and a Freescale MPL115A1 barometer (Freescale Semiconductor Inc. 2011).

c. Mechanical

The current design uses a low-cost approach. The batteries and controller are contained in a commercially available plastic case (''Pelican Case'' type) with a single hole and gland for the sensor cable to exit. The contents of the case are held in position using ''rip out'' foam inserts. This approach is low cost, simple, and works well. However, there are concerns that snow build up on the top can affect antenna performance. Also, the cases are not buoyant, so the case will not perform well if a melt pond forms around it. A typical deployment is shown in Fig. 2.

FIG. 2. Deployment of a typical system. The chain is being fed down a 2-in. hole and already has a weight attached to the bottom. The electronics is housed in the case to the right. The upright pole will hold a section of the chain in the air.

To extend the lifetime of deployments, a large floating hull has been developed and deployed but is still the subject of refinement. This consists of three rigid plastic tubes of 10-cm diameter and 5-m length formed to surround a sensor chain. A box on top contains the controller and the bases of the tubes are ballasted with batteries so the whole unit floats upright with the top of the sensor chain above water level. This can be deployed in a 10-in. hole and floats freely when the ice breaks up. A deployment of such a device is shown in Fig. 3. These are capable of monitoring ice formation, since they can be deployed in open water in the autumn months. However, their cost is significantly more than the standard SAMS IMB buoy in both construction and transportation.

4. Accuracy and calibration

The Maxim DS28EA00 sensor device used has a resolution of 1/16th (0.0625) of a degree Celsius and a stated

FIG. 3. Deployment of a floating system. The device is about to be lowered into a 10-in. hole. The sensor chain runs down the center of the structure surrounded by the three long sections of tube. The box on top holds the controller, and batteries are internal at the base of the three tubes to act as ballast. The buoy will float upright, such that the top 30 cm of the chain are above the water surface.

accuracy of ±0.5°C in an operating range of 85°C down to −10°C (Maxim Integrated 2009). The device will also operate from −10° to −40°C but at a reduced accuracy of from −0.5° to +2.0°C. The data sheet accuracy figures for the colder range are based on design calculation and not empirical measurement as is the case for the warmer range. Our own experiences suggest the −10°C error figures are pessimistic, since we do not observe large random variations in lengths of adjacent sensors that are exposed to the same low temperatures. The manufacturer does not indicate what portion of error can be attributed to offset or nonlinearity.

To correct any offset error, the temperature sensors are calibrated with a single-point calibration after assembly onto the completed chain. The chain is immersed in a precision temperature-controlled water bath at 1°C with a high-quality calibrated reference thermometer (Fluke Corp., model 1504). Any observed offset is stored for each device in the electrically erasable programmable read-only memory (EEPROM) mounted on the chain. The digital quantization error is half a least significant bit (LSB), or ±31.25 m°C, and is a random error. In addition, the reference thermometer accuracy of ±2 m°C represents a systematic error. Figures for any possible nonlinearity in the sensor temperature response are not available and have not yet been measured by ourselves.

The sensor data sheet suggests drift can be as large ±0.2°C. However, this figure represents results from tests on "another comparable device" and under stress tests for 1000 h in conditions designed to produce maximum drift (i.e., elevated temperatures of +85°C and continually powered). The deployment conditions are much more benign (normally no power applied and cold). We have had access to unpublished manufacturers' data on the actual device used that suggest the drift is minimal (98% below 1 LSB, i.e., no change in ADC count) even in stressed conditions. However, since the tests are unrepresentative of our applications and detailed results are not generally published, we intend to conduct our own drift tests in deployment conditions. Sensor readings from long-term deployments of chains in the Antarctic mixed layer beneath growing sea ice (where the temperature is expected to be maintained very close to the freezing point over considerable depth) suggest that random sensor drift is lower than the manufacturers stated ±0.2°C. In such situations no drift is readily apparent within lengths of adjacent sensors. However, to properly quantify the drift errors a full experimental study is still required.

Overall, the accuracy of the SAMS IMB buoy is comparable with the CRREL IMB buoy, which has a stated accuracy of ±0.1°C and which seems acceptable to the user community for ice mass balance studies.

No work has yet been published on attempts to use the results from the SAMS IMB buoy device for calculation of heat fluxes, and so it is not yet understood how the errors will influence the results of such work.

5. Heated operation mode

a. *Theory of operation*

The novel feature of this new IMB buoy is the development of chains that can be operated in what can be described as either a "hot-wire anemometer" mode or a needle-probe thermal conductivity mode. Hot-wire anemometry is a standard technique in experimental fluid dynamics and has been widely described (e.g., Perry 1982; La Barbara and Vogel 1976). Essentially a temperature-sensing element in a moving fluid is heated to above ambient temperature, and the amount of heat required to maintain a constant sensor temperature is measured. The amount of heat required depends on both the thermal characteristics of the surrounding fluid and its flow velocity. In principle, the output of the Maxim DS28EA00 sensor device can be refined for the estimation of both these quantities, thus allowing determination of the position of the ice–air–water interfaces and quantification of flow speeds. The sensitivity of the present design is not yet capable of the quantification of flow speeds.

Alternatively, the measurement principle is similar to that used for needle-probe thermal conductivity measurement in solids, such as those used in snow (Jaafar and Picot 1970; Sturm and Johnson 1992). In this case, heat is conducted away from the sensor chain at a rate dependent on the thermal properties of the material in which it is embedded.

With no heat applied to the sensor, the sensor will report a value $T = T_m$, where T_m is the temperature of the surrounding medium. Heat is introduced by applying an excitation voltage V to the resistor chip bonded to the sensor. All the resistor chips in the chain are of equal voltage R, are connected in parallel and experience the same excitation voltage, and generate the same heat $Q = V^2/R$. The temperature response of the sensor during heating will be a function of the geometry of the sensor and chain, the thermal diffusivity of the surrounding medium, and the flow rate of the medium (if a fluid).

For a traditional needle-probe measurement in a solid, the rise in temperature ΔT seen by the probe can be determined by

$$\Delta T = \frac{Q}{4\pi\lambda}[\ln(t_2) - \ln(t_1)], \tag{1}$$

where λ is the thermal conductivity of the surrounding material and $t_2 - t_1$ is the elapsed time during heating. Given the large differences in thermal conductivity between air, snow, ice, and water, the rise in temperature can be used to differentiate between these media. For the sensor chain, the geometry is somewhat different, and individual sensors may behave more as point sources than the cylindrical geometry in (1), which will change the proportionality constant.

There are various factors that make it impractical to use this idealized model to accurately determine thermal conductivity. These include the need for multiple measurements during the heating cycle to determine thermal conductivity accurately, the complex geometry of the chain and sensors causing the response to vary from a linear relationship and, especially, fluid flow around the sensor. Although accurate determination of thermal conductivity is not practical, discrimination of different layers within the air/snow/ice/ocean system is still possible—particularly for discriminating snow from ice.

When there is fluid flow (i.e., in air or water), the fluid will draw heat away from the sensor, so that (1) no longer applies. After an initial transient response, the temperature will reach a steady state determined by the balance of the heat input to the sensor and the speed of the fluid. In this case, the sensor will behave more like a hot-wire anemometer. In this mode, the observed temperature rise is best described by

$$\Delta T = \frac{Q}{HA}, \tag{2}$$

where H represents the heat transfer coefficient particular to the chip and surrounding media, and A is the effective area. For a normal hot-wire anemometer, the probe is typically a cylinder. Here, the geometry is more complex and the effective area is more difficult to determine. In this case, the term HA combines the effects of the sensor and chain geometry, the effects of the thermal properties of the chain and its surrounding medium, and the effects of the velocity of the medium. Heat transfer H is best described by an empirical relationship of the form

$$H = a + bv^c, \tag{3}$$

where v is fluid velocity and a, b, and c are constants determined by various system parameters; c typically has a value of ~0.5 (King's law; King 1914). Given that values of v are likely to vary over time scales that are much shorter than changes in the location of the ice–air and ice–water interfaces, it may be possible to both delineate these interfaces and make estimates of flow velocity as a function of time. In practice, we have found that discrimination between snow and ice at the snow surface, and ice and water at the ice–water interface is difficult using differences in the temperature rise alone. In this case, however, temporal variations in the temperature rise given by (2) and (3) due to variations in fluid velocity can be used to reliably identify these interfaces.

b. Heat cycle empirical characterization

The sensor chains have been tested in simulated sea ice conditions in a cold room (minimum temperature is −40°C) to determine the heating cycle response. Ice was grown in open-topped insulated boxes with heating pads at the bottom. This arrangement ensured ice growth occurred from the surface downward in a uniform sheet. A chain was suspended into the box before freezing, such that it had sections in air, ice, and water. The ice thickness was manually measured by drilling small holes into the ice and inserting a graduated hooked rod to feel for the underside.

The change in temperature was detected by each sensor along the chain for a heating period of 2.5 min. In water and ice, the temperature rise quickly approaches a near steady state for a 50% duty cycle (31 mW) as shown in Fig. 4. Heating continues for longer at 100% duty cycle (63 mW), providing clearer separation in saturation temperature between air and water (Fig. 5). In either case, the temperature response in water and ice does not follow a logarithmic curve as predicted by (1). Instead, the temperature approaches a saturation point

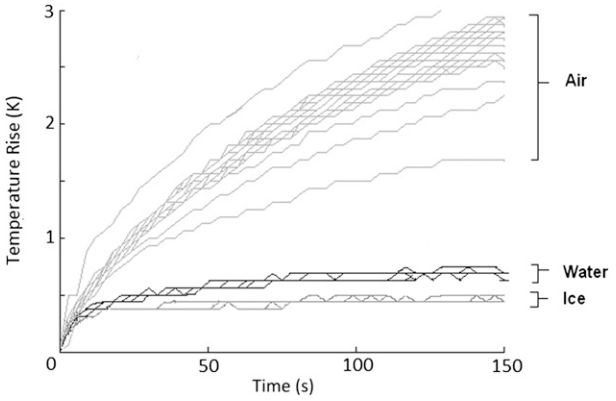

FIG. 4. Temperature rise of sensors during the heating cycle at 50% duty cycle (32 mW).

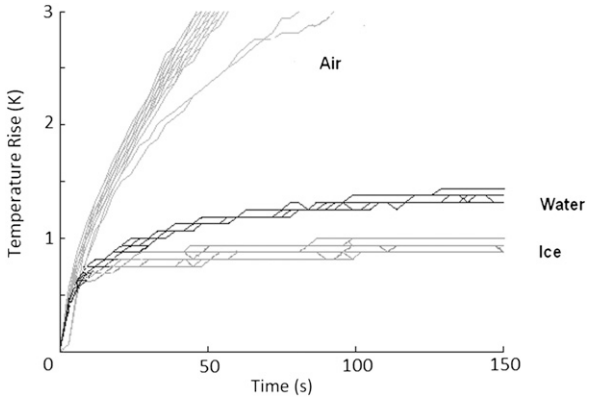

FIG. 5. Temperature rise of sensors during the heating cycle at full power (64 mW).

where further heating produced little increase. This might reflect initiation of a hot-wire anemometer mode in water, but it cannot explain the behavior in ice. It is presumed that the nonideal geometry of the sensor chain–ice system is responsible (i.e., it is not the point source as modeled by the equations) and additional heating is dissipated by conduction along the chain itself. In air, heating provided a clear distinction with water or ice, but the behavior is not logarithmic here either, instead rising more linearly. This probably reflects the significant thermal mass of the chain relative to the surrounding air. This suggests that in the present configuration, precise determination of material properties is difficult, but media are distinguishable empirically.

For the case of an ice–water interface, identification of the boundary may be difficult based on heating cycle information alone. For the lower level of heating applied in Fig. 4, the distinction amounts to only a few sensor resolution steps. While this difference can be increased by using greater heating power, this will come at the cost of battery lifetime (an estimated reduction of 25% to double the temperature interval).

The controlled tests described above represent a steady-state environment. In field deployments the sensors in air and water will be subject to a varying flow that greatly affects the temperature rise. Given the similar responses of the sensors in static water and ice, this mechanism may be significant in helping to distinguish the two media.

Figure 6 shows the measured heat rise at 63 mW for a sensor in a flume with a controlled water flow rate. Heating ceases after 150 s. While the sensor is sensitive to flow, the device saturates very quickly at very low flow rates and is unable to reliably differentiate between flow speeds above 2 cm^{-1}. This suggests that in static water, we can expect a temperature rise of about a 1.4°C and in heavily flowing water, a reduced temperature rise of about 0.7°C is expected. In ice the temperature rise also tends to be about 0.7°C. This could cause difficulties discriminating between ice and water in conditions of constant flow. However, in sea ice deployments, the flow rate of the fluid varies considerably over time being driven by tides and wind. It is this variation that permits identification of interfaces between materials with a similar thermal response (such as water and ice or snow and air) by monitoring this variation over a sequence of readings. This technique is described below in section 7.

The amount of data telemetered back from the heating cycle is minimized to reduce power consumption and data costs. At present two measurements are taken, one at the end of the heating cycle and one at an earlier point on the rising curve. Typically, the endpoint temperature is most useful since it shows the greatest temperature rise. In principle, additional readings during heating can be used to provide better determination of thermal

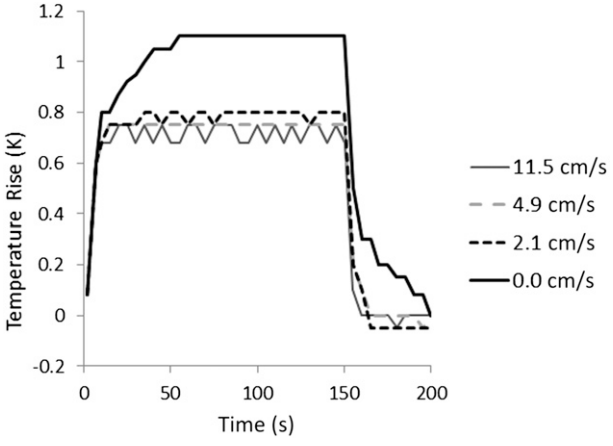

FIG. 6. Heat temperature rise of sensors in water during the heating cycle in different water flow rates.

conductivity or heat transfer coefficient, but the present analysis suggests that without careful calibration of the system, the penalty in terms of telemetry costs might outweigh any possible benefit of increased sampling.

6. Deployment

The SAMS IMB buoy devices are small, light, and easily deployed by personnel with minimal training. At present, the chain is fed through a hole in the ice and snow made with a standard 2-in. auger. A weight is attached to the bottom end to keep the chain straight down under the ice and a section above the ice is secured to a thin pole for snow detection and air temperature measurement. Data are relayed back after each sample using the Iridium SBD system as an e-mail attachment sent to a specified address. The incoming e-mail is processed automatically by a software server and the extracted data are stored in a database for subsequent analysis. A web server also displays the latest results and engineering data for monitoring purposes.

During deployment, manual measurements of snow and ice thickness and freeboard are taken and the positions of the sensors relative to the interfaces are noted so that the initial state is known. One weakness of the SAMS IMB buoy is the deployment disturbs the snow–ice system. This is particularly true for the snow, which may have poor contact with the chain if the hole is not carefully drilled and refilled. If the ice has positive freeboard, then the top section will be air or snow filled. As the hole refreezes, this air gap will be left but may subsequently fill with snow or flood and refreeze. In summer, the presence of the chain through the snow may cause increased solar energy absorption and speed the melt of the snow. Further tests of the effect of the physical presence of the IMB buoy are warranted.

7. Performance of deployments

To date, about 50 SAMS IMB buoy deployments have been made by 12 different institutions. Many of the first Arctic deployments were short lived because the ice floes quickly disintegrated (often corroborated by other instrumentation in the same place failing at the same time), but they still often revealed interesting information on the rapid melting that occurred before breakup. Wildlife also presents a risk to deployments and the destruction of one by a polar bear was witnessed in Svalbard, Norway. However, a number of deployments have fared better and lasted for periods in excess of a year.

An example of data from a deployment in the Weddell Sea in Antarctica is shown in Fig. 7. This deployment was made in ice of about 110 cm thick with about 8 cm of snow initially. The deployment was made in January and drifted for over a year before the ice in the floe on which it was deployed melted in the northern Weddell Sea. Note that as it was initially deployed through a large hole (significantly bigger than the 2-in. hole normally used), the chain took much longer to freeze before the freezing front apparent in Fig. 7 actually passed the initial ice–ocean interface (around day 100). Figure 7a shows the temperature evolution starting in air at the top, within the ice and snow, and then the upper ocean. The white lines are the estimated positions of the air–snow, snow–ice, and ice–ocean interfaces estimated by inflection points in the vertical temperature profile. The top ice surface is used as the zero depth reference. It is not possible to reliably identify the interfaces from the temperature profiles alone.

The heating cycle temperature rise clearly delineates the snow–ice boundary (Fig. 7b) as expected because of the differences in thermal conductivity. If a form of (1) held, then we would expect the heating rate to be proportional to the inverse of the effective thermal conductivity. These results suggest an apparent thermal conductivity for ice about twice that of the snow, while in reality it is about 5–7 times. This clearly shows that (1) does not hold. One possible contributing factor is that the heating in snow saturates quickly as convection is initiated, as noted by others (Sturm and Johnson 1992).

The boundaries between air and snow and between ice and water are not clearly identifiable from observation of the heating rates in situations where fluid flow reduces the distinction between lower-conductivity fluids (e.g., water) and higher-conductivity solids (e.g., ice). However, as described above, the data can be processed to make the interfaces more obvious. One approach is to take the ratio of the temperature rise during the heating cycle at two instances. A point approximately midway up the rising temperature curve and a point nearing saturation were sought so sample times at 15 and 60 s were used (Fig. 7c—note here it is actually the natural logarithm of this ratio that is shown, as this emphasizes the interfaces more clearly). This approach still shows a clear snow–ice boundary, but it also provides a clearer discrimination between the air–snow and ice–ocean interfaces.

An alternative approach is to examine the deviation of the heating rate for each sensor over the course of several adjacent samples. A ''box-car type'' filter covering five sample periods has been used to achieve the background average against which the deviation of a sample is measured. The choice of five samples is arbitrary, and it is noted that using longer periods seems to

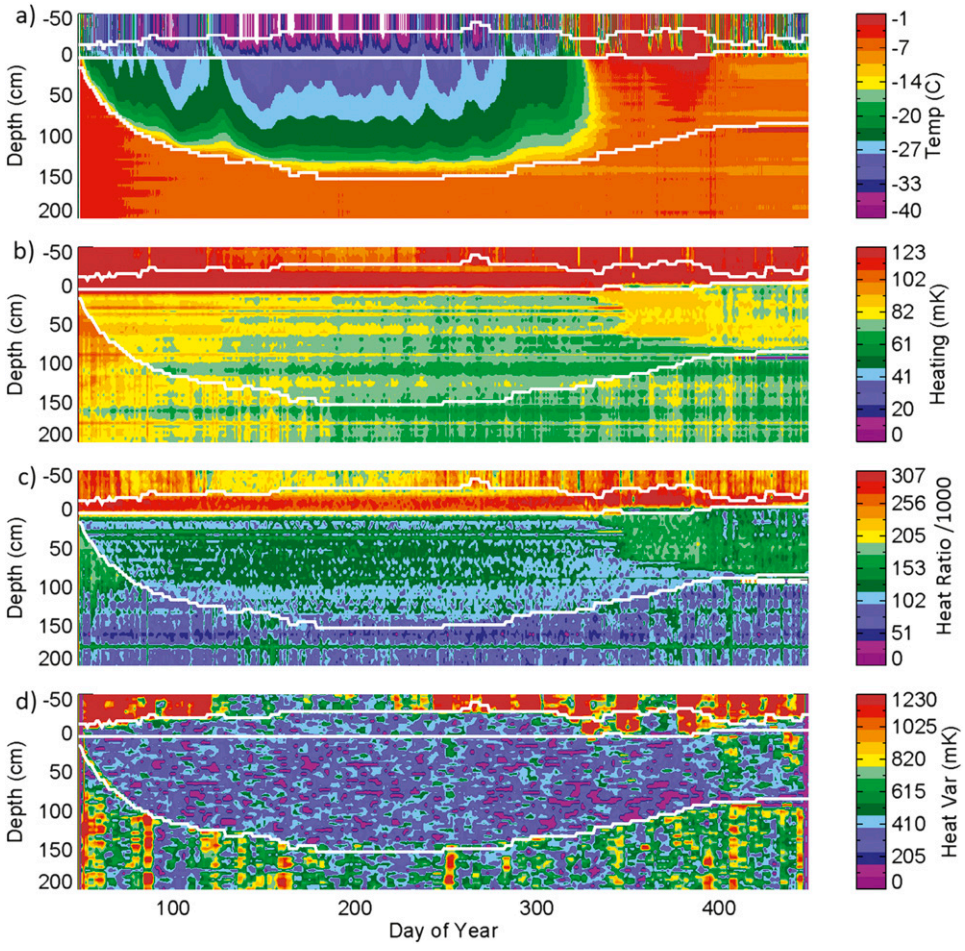

FIG. 7. Results from a typical deployment made in the Antarctic in midsummer. (a) Temperature evolution from top of chain through ice down into water. (b) Temperature rises after heating for 60 s. (c) Natural logarithm of the ratio of temperatures rises at 15- and 60-s points during a heating cycle. (d) Variation of each sample from local average (i.e., current sample and two samples either side in time). The white lines represent manual estimation of interfaces from inspection of the vertical temperature profiles only, providing an independent validation of the ability of the heating cycle to identify the interfaces.

cause little difference to the results. The filter is centered on the sample for which the deviation is being calculated, so as not to introduce temporal shifting. The variation in heating rate due to variations in the flow rate becomes very obvious (Fig. 7d). Here, the air–snow and ice–ocean interfaces can be readily picked out because of the temporal variations in heating of sensors in the fluids (presumably primarily due to variations in flow rates of the fluids).

Later in the deployment (days 350–450), it would appear there are some internal changes apparent within the ice where higher temperatures in response to the applied heating occur. This remains unexplained as yet, but it is thought that it may be due to increasing porosity of the ice during melting conditions. Similar patterns have been noted previously (Polashenski et al. 2011).

8. Validation of performance

A SAMS IMB buoy and a CRREL IMB buoy were deployed together in a frozen lake in Alberta in the winter of 2009/10 to validate the performance of the SAMS device with regard to its ability to detect different media using the heating mode. The CRREL device uses ultrasound ranging to detect interfaces and is field proven so it is used in this situation as a reference. The location of the lake also permitted regular visits, so that manual measurements could be made to validate both devices over the winter months while the lake remained frozen. Results are plotted in Fig. 8, and some statistical analysis results are presented in Table 1.

This experiment used a short (60 s) heating cycle, which has now been recognized as too short to optimally

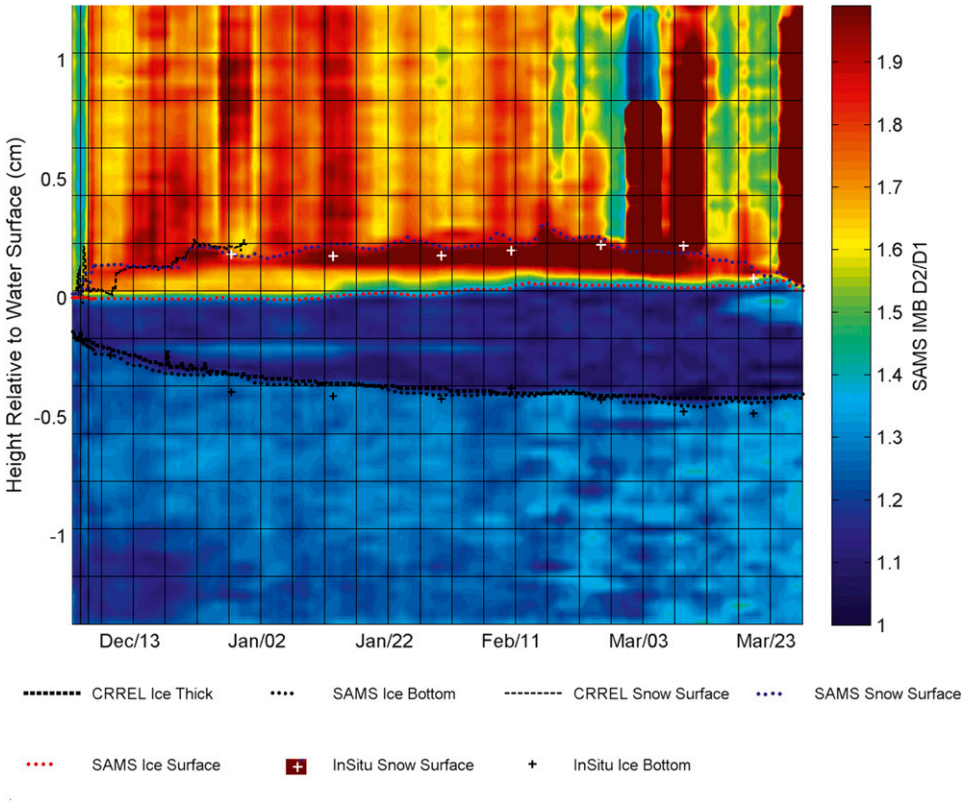

FIG. 8. Results of CRREL and SAMS IMB buoy comparative deployment. For the SAMS device, the colors represent the ratio of temperature rises after 15 and 60 s of heating (D2/D1). From this the interfaces have been plotted manually by eye. The traces for the CRREL IMB buoy are plotted directly. Periodic manual (in situ) measurements are also plotted as discrete points.

discriminate the ice–water interface but is still adequate. To accentuate the interfaces, these data were processed to highlight differences in heating rise time. The temperature rise in this case was sampled at 15 and 60 s, and the ratio of these are determined and plotted in Fig. 8. Since there is little or no current variation present in a lake, the ice–water interface is not as clearly visible as it might be in a sea ice deployment. Note that a deliberate step reduction in heating power of 50% at 10 weeks is compensated and is not clearly visible using this processing method. This suggests the heating curve rise-time coefficient is insensitive to heating power, since the ratio between two fixed time samples on the curve remains the same.

Using manually fitted curves for the SAMS IMB buoy data, the results from both buoys can be compared and are plotted in Fig. 9. This plot also shows results from periodic manual measurement of interface positions. Note that the CRREL snow depth sensor failed after four weeks, which limited the comparison. A statistical comparison detailed in Table 1 shows good correlation between the buoys. It should be noted that the SAMS thermistor chain used in this instance had sensors at 4-cm separation instead of the more usual 2-cm separation now routinely used. For comparison, the ultrasonic range sensors used in the CRREL buoy claim an accuracy of ±1 cm above the ice (Cambell Scientific SR-50) and a resolution of 1 cm below the ice (Benthos PSA-916).

9. Conclusions and further work

The SAMS IMB buoy has been developed and deployed over 50 times in sea ice in both polar regions.

TABLE 1. Comparison of results from CRREL ultrasonic mode and SAMS hot-wire mode IMB buoys.

	(CRREL − SAMS) (cm)	
	Snow	Ice
No. of points	124	37
Mean difference	−5.0	−3.3
Std dev difference	1.7	5.3
Median difference	−1.0	−2.8
Max difference	8.2	12.7
Min difference	−4.0	−10.9

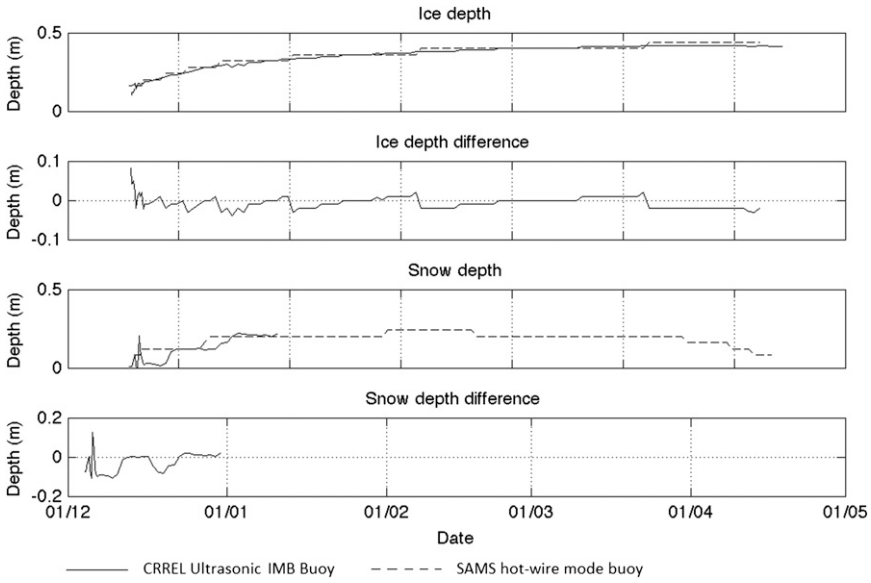

FIG. 9. Comparison of results from ultrasonic CRREL buoy and hot-wire mode SAMS buoy both deployed side by side on a frozen lake. The interfaces for the SAMS buoy have been manually derived from visual interpretation. The CRREL snow depth sensor failed after four weeks.

The use of a single chain of solid-state sensors with heating elements has provided a low-cost, easily deployable alternative to more expensive systems. Ice growth and decay and snow accumulation and ablation can be determined using heating elements on the sensors via the principle of thermal conductivity or hot-wire anemometer measurements. Some processing of the data is necessary to clearly delineate the interfaces in all cases, and under some conditions, discrimination may not be entirely clear, which could cause a loss of resolution compared to acoustic sensing of the interfaces. There remains the possibility that the physical presence of the chain may impact measurements, particularly in the melt season. On the other hand, recent deployments have lasted for more than a year and have returned clear and useful data, demonstrating the durability and reliability of the device. Moreover, the ability to detect possible changes in thermal properties at each sensor allows the possibility of identifying internal changes in the ice and snow. Despite potential weaknesses, the low cost makes it feasible to deploy large numbers of the device, so that a more complete picture of sea ice mass balance processes may be possible.

There is still significant scope for development and refinement in all aspects of the device, including its design, operation, and the processing of results. The most urgent work is to properly characterize the chains such that their accuracy, drift, and performance of the heating mode can be better understood. It is hoped that with more characterization data, the postprocessing software can be modified to automatically detect interfaces, identify the medium local to a sensor and also produce measurements of air and water currents. Better characterization could also help optimize the design. Continuing effort is also being made to improve the method of chain construction.

Other related work includes making the chains much longer (at least 100 m) so that useful data on heat fluxes in the upper layers on the ocean can be measured. The spacing of sensors can be increased for this purpose and the need for heating is not necessary. The incorporation of depth sensors into the chain using the single-wire bus is also underway.

Acknowledgments. The original development of the SAMS IMB buoy was funded by the Natural Environment Research Council (NERC) of the United Kingdom under a project called ''Novel Ice Characterisation Experiment – 1'' (NICE-1). Refinements were made possible through the NERC ASBO, ICEBELL and TEA-COSI projects as well as EU-funded DAMOCLES and ACCESS programs and the Office of Naval Research's Marginal Ice Zone DRI program. Commercial development, marketing, and sales of the device has been supported by SAMS Research Services Ltd. (SRSL). Figure 3 is by Peter Bucktrout of the British Antarctic Survey.

REFERENCES

Ackley, S. F., C. H. Fritsen, V. I. Lytle, and C. W. Sullivan, 1996: Freezing driven upwelling in Antarctic sea ice biological systems. *Proc. NIPR Symp. Polar Biol.,* **9,** 45–59.

Flower, G. A., and G. Budgen, 1987: The development of thermistor chain buoys for use in ice infested waters. *OCEANS '87 Proceedings: The Ocean—An International Workplace,* Vol. 1, IEEE, 220–224.

Freescale Semiconductor Inc., 2011: Miniature SPI digital barometer. Data Sheet Doc. MPL115A1, Revision 6, 15 pp. [Available online at http://www.datasheetarchive.com/1–MPL115A1-datasheet.html#.]

Haas, C., S. Hendricks, H. Eicken, and A. Herber, 2010: Synoptic airborne thickness surveys reveal state of Arctic sea ice cover. *Geophys. Res. Lett.,* **37,** L09501, doi:10.1029/2010GL042652.

iButtonLink, LLC, 2008: The LinkOEM module: Users guide. Revision 1.2, iButtonLink LLC, 10 pp. [Available online at http://cdn.shopify.com/s/files/1/0164/3524/files/LinkOEM_Users_Manual_V1_2.pdf?1957.]

Iridium Communications Inc., 2010: Iridium 9602 technical brochure. Iridium, 2 pp. [Available online at http://www.iridium.com/products/Iridium9602.aspx?section=support.]

Iridium Satellite, LLC, 2012: Iridium 9603 brochure. Iridium, 4 pp. [Available online at http://www.iridium.com/products/Iridium-9603.aspx?section=support.]

Jaafar, H., and J. J. C. Picot, 1970: Thermal conductivity of snow by a transient state probe method. *Water Resour. Res.,* **6,** 333–335, doi:10.1029/WR006i001p00333.

King, L. V., 1914: On the convection of heat from small cylinders in a stream of fluid: Determination of the convection constants of small platinum wires, with applications to hot-wire anemometry. *Phil. Roy. Soc. London,* **A90,** 563–570.

Kwok, R., H. J. Zwally, and D. Yi, 2004: ICESat observations of Arctic sea ice: A first look. *Geophys. Res. Lett.,* **31,** L16401, doi:10.1029/2004GL020309.

——, G. F. Cunningham, S. S. Manizade, and W. B. Krabill, 2012: Arctic sea ice freeboard from IceBridge acquisitions in 2009: Estimates and comparisons with ICESat. *J. Geophys. Res.,* **117,** C02018, doi:10.1029/2011JC007654.

La Barbara, M., and S. Vogel, 1976: An inexpensive thermistor flowmeter for aquatic biology. *Limnol. Oceanogr.,* **21,** 750–756.

Laxon, S., N. Peacock, and D. Smith, 2003: High interannual variability in sea ice thickness in the Arctic region. *Nature,* **425,** 947–950.

Maxim Integrated, 2007: Regain location information by leveraging the 1-wire chain function—A simple signaling and protocol method determines device physical location. Maxim Integrated Application Note 4037, 7 pp.

——, 2009: 1-wire digital thermometer with sequence detect and PIO. DS28EA00 Data Sheet, Revision 2, Maxim Integrated, 29 pp.

Microchip Technology Inc., 2010: PIC24FJ256GA110 family data sheet. Microchip Technology, 330 pp. [Available online at http://ww1.microchip.com/downloads/en/DeviceDoc/39905e.pdf.]

Mobley, F. F., A. C. Sadileck, C. J. Gundersdorf, and D. Speranza, 1976: A new thermistor chain for underwater temperature measurement. *OCEANS '76,* IEEE and MTS, 529–536.

Perovich, D. K., B. C. Elder, K. J. Claffey, S. Stammerjohn, R. Smith, S. F. Ackley, H. R. Krouse, and A. J. Gow, 2004: Winter sea-ice properties in the Marguerite Bay region. *Deep-Sea Res. II,* **51,** 2023–2039, doi:10.1016/j.dsr2.2004.07.024.

——, J. A. Richter-Menge, K. F. Jones, and B. Light, 2008: Sunlight, water, and ice: Extreme Arctic sea ice melt during the summer of 2007. *Geophys. Res. Lett.,* **35,** L11501, doi:10.1029/2008GL034007.

Perry, A. E., 1982: *Hot-Wire Anemometry.* Oxford University Press, 184 pp.

Persistor Instruments Inc., 2005: Persistor CF2: Getting started guide. Rev. 2.0, Persistor Instruments, 30 pp. [Available online at http://www.persistor.com/doc/cf2/cf2gsg.pdf.]

PNI Sensor Corp, 2010: MicroMag user manual. PNI Sensor Corp., 23 pp. [Available online http://www.pnicorp.com/support/files/micromag-user-manual.]

Polashenski, C., D. K. Perovich, J. A. Richter-Menge, and B. Elder, 2011: Seasonal ice mass-balance buoys: Adapting tools to the changing Arctic. *Ann. Glaciol.,* **52** (57), 18–26.

Richter-Menge, J. A., D. K. Perovich, B. C. Elder, K. Claffey, I. Rigor, and M. Ortmeyer, 2006: Ice mass balance buoys: A tool for measuring and attributing changes in the thickness of the Arctic sea ice cover. *Ann. Glaciol.,* **44,** 205–210.

Rothrock, D. A., Y. Yu, and G. A. Maykut, 1999: Thinning of the Arctic sea-ice cover. *Geophys. Res. Lett.,* **26,** 3469–3472.

——, J. Zhang, and Y. Yu, 2003: The Arctic ice thickness anomaly of the 1990s: A consistent view from observations and models. *J. Geophys. Res.,* **108,** 3083, doi:10.1029/2001JC001208.

Scott, J. C., and A. L. McDowall, 1990: Cross-frontal cold jets near Iceland: In-water, satellite infrared, and Geosat altimeter data. *J. Geophys. Res.,* **95** (C10), 18 005–18 014.

Sellschopp, J., 1997: A towed CTD chain for two-dimensional high resolution hydrography. *Deep-Sea Res. I,* **44,** 147–165.

Smith, M., 2004: IC thermal sensors: Simplify your design. *Sensors Mag.,* **21** (11). [Available online at http://archives.sensorsmag.com/articles/1104/14/.]

Strass, V. H., 1997: Measuring sea ice draft and coverage with moored upward looking sonars. *Deep-Sea Res.,* **45,** 795–818.

Sturm, M., and J. B. Johnson, 1992: Thermal conductivity measurements of depth hoard. *J. Geophys. Res.,* **97** (B2), 2129–2139.

U-blox AG, 2013: UP501 Fastrax GPS patch antenna module data sheet. Doc. FTX-HW-12010-B1, 2 pp. [Available online at http://www.u-blox.com/images/downloads/Product_Docs/UP501_ProductSummary_%28FTX-HW-12005%29.pdf.]

Untersteiner, N., 1961: On the mass and heat budget of Arctic sea ice. *Arch. Meteor. Geophys. Bioklimatol.,* **A12,** 151–182.

Wadhams, P., and N. R. Davis, 2000: Further evidence of ice thinning in the Arctic Ocean. *Geophys. Res. Lett.,* **27,** 3973–3975.

Wilkinson J. P., P. M. Wadke, D. Meldrum, D. Mercer, M. Doble and P. Wadhams, 2007: The autonomous measurement of waves propagating across the Arctic Ocean. *Proc. OCEANS 2007,* Vancouver, BC, Canada, MTS/IEEE, doi:10.1109/OCEANS.2007.4449329.

Worby, A. P., M. O. Jefferies, W. F. Weeks, K. Morris, and R. Jana, 1996: The thickness distribution of sea ice and snow cover during late winter in the Bellingshausen and Amundsen Seas, Antarctica. *J. Geophys. Res.,* **101** (C12), 28 441–28 445.